ON FULLY DISCRETE SCHEMES FOR THE FERMI PENCIL-BEAM EQUATION

MOHAMMAD ASADZADEH AND ALEXANDROS SOPASAKIS

ABSTRACT. We consider a Fermi pencil beam model in two space dimensions (x, y), where x is aligned with the beam's penetration direction and y together with the scaled angular variable z, correspond to a bounded symmetric, transversal cross section. We study some fully discrete numerical schemes using the standard Galerkin and streamline diffusion finite element methods for discretization of the transversal domain combined with backward Euler, Crank-Nicolson and discontinuous Galerkin methods for discretization in the penetration variable. We derive stability estimates for the semidiscrete problems and, assuming sufficiently smooth exact solution, we show optimal a priori error estimates. Numerical examples presented in some canonical cases, with data approximating Dirac δ function, confirm the expected performance of the combined schemes.

1. INTRODUCTION

The Fermi pencil beam equation is derived from the Fokker-Planck equation through an asymptotic expansion. The Fokker-Planck equation itself is yet another asymptotic limit of the linear Boltzmann equation, see [6]. The assumption of *forward-peaked scattering*, in a transport process, comprises the back-bone of the derivation of both equations.

We study some fully discrete schemes for the numerical solution of a pencil beam model in two space dimensions. Introducing a scaled angular variable z, our model problem would correspond to a, degenerate type, convection dominated convection-diffusion problem in a slab of thickness L, $x \in I_x := [0, L]$, with a symmetric cross section $I_\perp := I_y \times I_z := [-y_0, y_0] \times [-z_0, z_0]$, for $y_0,\ z_0 \in \mathbb{R}^+$. Thus the physical domain, $I_x \times I_\perp$, is now three dimensional and the corresponding Fermi equation is modeling the penetration (in the direction of the x-axis) of narrowly focused pencil beam particles incident at the transversal boundary of an *isotropic* slab at the point $(x, y, z) = (0, 0, 0)$. The forward-peakedness assumption would allow us to consider bounded, convex transversal domain. For the isotropic background media we may assume that all involved functions are symmetric, more precisely *even functions*, in y and z.

In this setting, our model problem is thus formulated as follows: given the incident source intensity f at $x = 0$, find the current function u defined on the domain

1991 *Mathematics Subject Classification.* 65N15, 65N30, 35L80.

Key words and phrases. Fermi, Pencil beam, standard Galerkin, streamline diffusion, fully discrete schemes.

The second author is also affiliated with Texas A&M University.

$\Omega := I_x \times I_\perp$ satisfying the Fermi equation

$$(1.1)\quad \begin{cases} u_x + z u_y = \varepsilon u_{zz}, & \text{in } \Omega = I_x \times I_\perp, \\ u_z(x,y,\pm z_0) = 0, & \text{for } (x,y) \in I_x \times I_y, \\ u(0,x_\perp) = f(x_\perp), & \text{for } x_\perp \in I_\perp, \\ u(x,x_\perp) = 0, & \text{on } \Gamma^-_{\tilde\beta} = \{(x,x_\perp) \in \Gamma := \partial\Omega,\ \tilde{\mathbf{n}} \cdot \tilde\beta < 0\}, \end{cases}$$

where $z = \tan(\theta)$, $-\pi/2 < \theta < \pi/2$, corresponds to scaled angular variable, $x_\perp := (y,z)$ and $2\varepsilon = \sigma_{tr}(x,y)$. Here $\sigma_{tr}(x,y) \sim 1/l$, ($l$ is the mean free path), the transport cross section, is a positive small and decreasing function of (x,y) indicating energy deposit due to particle collisions. Finally $\tilde\beta = (1,z,0)$ and $\tilde{\mathbf{n}} := \tilde{\mathbf{n}}(x,x_\perp)$ is the outward unit normal to Γ at $(x,x_\perp) \in \Gamma$. As we stated earlier this model problem corresponds to a convection dominated (ε small) convection-diffusion problem which can be interpreted as a time-dependent (with x corresponding to the time variable) convection-diffusion problem of degenerate type (convection in y, diffusion in z).

For this type of equation the usual standard Galerkin scheme would converge very slowly. Even for the non-degenerate convection dominated problems, having hyperbolic nature, the standard finite element schemes would have poor convergence behavior, of order $O(h^k)$ versus $O(h^{k+1})$ for elliptic and parabolic problems (assuming the exact solution in the Sobolev space H^{k+1}, and a quasi-uniform triangulation, with mesh size h), see [9]. The idea of including artificial viscosity term, e.g. by adding some amount of diffusion in the equation, is to improve this poor behavior and speed up the convergence of standard finite elements for hyperbolic type problems. Here, the streamline diffusion method would automatically add a proper amount of extra viscosity term through a modified form of the test function.

Some related studies of the Fokker-Planck and Fermi pencil beam models can be found in [2], [3] and [4]. In [2] *a priori* error estimates are derived for the fully discrete problems using the streamline diffusion and discontinuous Galerkin methods, while [3] is devoted to the *a posteriori* error estimates in the same setting. *Characteristic* methods, based on the technique of *exact transport + projection*, are considered in [4].

Below first we study the semidiscrete schemes where we discretize in the transversal variable $x_\perp =: (y,z)$, using the standard Galerkin (=SG) and streamline diffusion (=SD) finite element methods with *weakly imposed boundary conditions*, and derive some stability estimates. Further, for the SG-method, assuming the exact solution being in the Sobolev space H^{k+1}, we also derive optimal a priori error estimates of order $O(h^k)$ in a L_2 based norm. While the corresponding convergence rate for the SD finite element method is $O(h^{k+1/2})$, as shown in [2]. Our convergence results in the semidiscrete part are based on Galerkin orthogonality and strong stability estimates derived for certain bilinear forms. These are the usual approaches studied for the standard problems which we have extended to a degenerate type equation.

As for the fully discrete problem: because of the structure of the equation here the penetrating variable x is interpreted as a time variable and therefore appropriately treated by the time discretization techniques such as: discontinuous Galerkin, backward Euler or Crank-Nicolson methods.

One of the basic applications of the Fermi pencil beam models is in the *dose* calculations of radiative cancer therapy, see [8]. Our computational results, in concrete examples, are useful in investigating the credibility of different numerical

algorithms proposed in this context. We present fast and efficient deterministic schemes competitive with the commonly used stochastic algorithms (with the additional advantage of having more reliably justified convergence rates than those in the stochastic approaches).

An outline of this paper is as follows: we start by presenting the semidiscrete approximation by the standard Galerkin finite element method in Section 2, prove a stability result for this type of discretization in Subsection 2.1 and derive the error estimates in Subsection 2.2. The corresponding investigations using the streamline diffusion approximation are presented in Section 3. Section 4 is devoted to fully discrete algorithms. Numerical simulations, for some relevant examples, together with the study of the behavior of either discretization algorithms are introduced in Section 5. Finally in Section 6 we comment on our results and outline a future work. Throughout the paper C will denote an absolute constant unless otherwise explicitly stated.

2. THE STANDARD GALERKIN METHOD

In this section we have a discretization in $x_\perp = (y, z)$ using the finite element approximation based on a quasi-uniform triangulation of the rectangular domain $I_\perp = I_y \times I_z$ with a mesh size h. To this approach we let $\beta = (z, 0)$ and define the inflow (outflow) boundary as

$$\Gamma_\beta^{-(+)} := \{x_\perp \in \Gamma := \partial I_\perp : \mathbf{n}(x_\perp) \cdot \beta < 0 (> 0)\}, \tag{2.1}$$

where $\mathbf{n}(x_\perp)$ is the outward unit normal to the boundary Γ at $x_\perp \in \Gamma$. Now we use the notation $v_z(\cdot) := \frac{\partial v}{\partial z}(\cdot)$ and introduce a discrete, finite dimensional, function space $V_{h,\beta} \subset H_\beta^1(I_\perp)$ with,

$$H_\beta^1(I_\perp) = \{v \in H^1(I_\perp) : v_z(\pm z_0) = 0, \quad \text{and} \quad v = 0 \ \text{ on } \ \Gamma_\beta^-\}, \tag{2.2}$$

such that, $\forall v \in H_\beta^1(I_\perp) \cap H^r(I_\perp)$,

$$\inf_{\chi \in V_{h,\beta}} \|v - \chi\|_j \le C h^{\alpha - j} \|v\|_\alpha, \quad j = 0, 1 \ \text{ and } \ 1 \le \alpha \le r, \tag{2.3}$$

where for positive integer s, $\|\cdot\|_s$ denotes the L_2-based Sobolev norm of functions with all their partial derivatives of order $\le s$, in L_2, see Adams [1]. An example of such $V_{h,\beta}$ is a set of sufficiently smooth piecewise polynomials $P(x_\perp)$ of degree $\le r$, satisfying the boundary conditions given in (2.2).

Now the objective is to find $u_h \in V_{h,\beta}$, such that

$$\begin{cases} (u_{h,x}, \chi)_\perp + (z u_{h,y}, \chi)_\perp + (\varepsilon u_{h,z}, \chi_z)_\perp = 0, \quad \forall \chi \in V_{h,\beta}, \\ u_h(0, x_\perp) = f_h(x_\perp), \end{cases} \tag{2.4}$$

where f_h is a finite element approximation of f and the mesh size h is related to ε according to:

$$h^2 \le \varepsilon \le h.$$

Here, $(u, v)_\perp = \int_{I_\perp} u(x_\perp) v(x_\perp)\, dx_\perp$ and $\|u\|_{L_2(I_\perp)} = (u, u)_\perp^{\frac{1}{2}}$. To distinguish, we use the following inner products notations: $(\cdot, \cdot)_\perp$ and $(\cdot, \cdot)_\Omega$, where $\Omega = [0, L] \times I_\perp = I_x \times I_\perp$, for integration over $I_\perp$ and $I_x \times I_\perp$, respectively.

2.1. **Stability.** In this part we prove a stability lemma in both inner products, $(\cdot,\cdot)_\perp$ and $(\cdot,\cdot)_\Omega$, to guarantee the control of the discrete solution by the data. For simplicity we introduce the triple norm,

$$|||v|||_{\tilde\beta}^2 = \frac{1}{2}\int_{\Gamma_{\tilde\beta}^+} v^2(\mathbf{n}\cdot\tilde\beta)\,d\Gamma + \|\varepsilon^{1/2}v_z\|_{L_2(\Omega)}^2, \tag{2.5}$$

where $\tilde\beta = (1,\beta)$ and $\Gamma_{\tilde\beta}^+ := \Gamma\setminus\Gamma_{\tilde\beta}^- = [0,L]\times\Gamma_\beta^+ \cup \{\{L\}\times I_\perp\}$.

Lemma 2.1. *For $u_h \in V_{h,\beta}$, satisfying (2.4) we have that,*

$$\sup_{x\in I_x}\|u_h(x,\cdot)\|_{L_2(I_\perp)} \leq \|f\|_{L_2(I_\perp)}, \tag{2.6}$$

$$|||u_h|||_{\tilde\beta}^2 = \frac{1}{2}\|u_h(0,\cdot)\|_{L_2(I_\perp)}^2. \tag{2.7}$$

Proof. We let $\chi = u_h$, in first equation, in (2.4) to obtain,

$$\frac{1}{2}\frac{d}{dx}\|u_h\|_{L_2(I_\perp)}^2 + (zu_{h,y},u_h)_\perp + \|\varepsilon^{1/2}u_{h,z}\|_{L_2(I_\perp)}^2 = 0. \tag{2.8}$$

Using integration by parts, in y, we may write

$$\begin{aligned}(zu_{h,y},u_h)_\perp =& \frac{1}{2}\int_{I_z} z\left(u_h^2(y_0)-u_h^2(-y_0)\right)\,dz\\ =& \frac{1}{2}\int_0^{z_0} z[u_h^2(y_0)-u_h^2(-y_0)]dz + \frac{1}{2}\int_{-z_0}^0 z[u_h^2(y_0)-u_h^2(-y_0)]dz\\ =& \frac{1}{2}\int_{\Gamma_\beta^+}(\mathbf{n}\cdot\beta)u_h^2\,d\Gamma,\end{aligned}$$

which, inserting in (2.8), gives that,

$$\frac{1}{2}\frac{d}{dx}\|u_h\|_{L_2(I_\perp)}^2 + \frac{1}{2}\int_{\Gamma_\beta^+}(\mathbf{n}\cdot\beta)u_h^2\,d\Gamma + \|\varepsilon^{1/2}u_{h,z}\|_{L_2(I_\perp)}^2 = 0. \tag{2.9}$$

Using (2.9) we shall obtain stability estimates for the semidiscrete problem, discretized by the SG-method (the corresponding continuous variational formulation would lead to similar stability estimates for the continuous problem). Now, since $\int_{\Gamma_\beta^+}(\mathbf{n}\cdot\beta)u_h^2\,d\Gamma \geq 0$, by (2.9), $\frac{d}{dx}\|u_h\|_{L_2(I_\perp)}^2 \leq 0$, i.e, $\|u_h\|_{L_2(I_\perp)}^2$ is decreasing in x and hence,

$$\|u_h(x,\cdot)\|_{L_2(I_\perp)} \leq \|f\|_{L_2(I_\perp)}, \quad \forall x\in[0,L]. \tag{2.10}$$

This gives the first statement of Lemma 2.1. Further, integrating (2.9) over $x\in[0,L]$ we get,

$$\frac{1}{2}\|u_h(L,\cdot)\|_{L_2(I_\perp)}^2 + \frac{1}{2}\int_0^L\int_{\Gamma_\beta^+}(\mathbf{n}\cdot\beta)u_h^2\,d\Gamma + \|\varepsilon^{1/2}u_{h,z}\|_{L_2(\Omega)}^2 = \frac{1}{2}\|u_h(0,\cdot)\|_{L_2(I_\perp)}^2.$$

Observe that the first two terms above amount to $\frac{1}{2}\int_{\Gamma_{\tilde\beta}^+}(\mathbf{n}\cdot\tilde\beta)u_h^2\,d\Gamma$, so that we obtain the second assertion of the Lemma and the proof is complete. □

Remark 2.1. Below we derive the corresponding pointwise version of Lemma 2.1: Let us consider $x' \in [0, L]$, integrating (2.9) over $(0, x')$, the procedure leading to the proof of the second assertion of the Lemma 2.1, would give,

$$\frac{1}{2}\int_{\Gamma^+_{\tilde{\beta},x'}} (\tilde{\mathbf{n}}\cdot\tilde{\beta})u_h^2\, d\Gamma + \|\varepsilon^{1/2}u_{h,z}\|^2_{L_2(\Omega')} = \frac{1}{2}\|u_h(0,\cdot)\|^2_{L_2(I_\perp)}, \tag{2.11}$$

where $\Gamma^+_{\tilde{\beta},x'} = \Gamma^+_{\tilde{\beta}} \times [0, x'] \cup \{\{x'\} \times I_\perp\}$ and $\Omega' = [0, x'] \times I_\perp$. Now since the right hand sides in (2.7) and (2.11) are identical and $\|\cdot\|^2_{L_2(\Omega')} \leq \|\cdot\|^2_{L_2(\Omega)}, (\Omega' \subseteq \Omega)$, thus

$$\int_{\Gamma^+_{\tilde{\beta}}} (\tilde{\mathbf{n}}\cdot\tilde{\beta})u_h^2\, d\Gamma \leq \int_{\Gamma^+_{\tilde{\beta},x'}} (\tilde{\mathbf{n}}\cdot\tilde{\beta})u_h^2\, d\Gamma, \tag{2.12}$$

or equivalently,

$$\int_0^L \int_{\Gamma^+_\beta} (\mathbf{n}\cdot\beta)u_h^2 d\Gamma + \|u_h(L,\cdot)\|^2_{L_2(I_\perp)} \leq \int_0^{x'} \int_{\Gamma^+_\beta} (\mathbf{n}\cdot\beta)u_h^2 d\Gamma + \|u_h(x',\cdot)\|^2_{L_2(I_\perp)}.$$

Evidently we also have for $x' \in [0, L]$,

$$\int_0^L \int_{\Gamma^+_\beta} (\mathbf{n}\cdot\beta)u_h^2\, d\Gamma \geq \int_0^{x'} \int_{\Gamma^+_\beta} (\mathbf{n}\cdot\beta)u_h^2\, d\Gamma, \tag{2.13}$$

thus,

$$\|u_h(L,\cdot)\|_{L_2(I_\perp)} \leq \|u_h(x',\cdot)\|_{L_2(I_\perp)}, \quad \forall x' \in [0, L]. \tag{2.14}$$

Generalizing (2.14), we have that the $L_2(I_\perp)$-norm of the finite element solution is decreasing in x, which also implies the first assertion of Lemma 2.1.

Below we state the continuous version of Lemma 2.1:

Corollary 2.2. *The solution u of problem (1.1) satisfies the stability relations,*

$$\sup_{x\in I_x} \|u(x,\cdot)\|_{L_2(I_\perp)} \leq \|f\|_{L_2(I_\perp)}, \tag{2.15}$$

$$|||u|||^2_{\tilde{\beta}} = \frac{1}{2}\|f\|^2_{L_2(I_\perp)}. \tag{2.16}$$

To proceed we introduce the bilinear form, $A : H^1_\beta(I_\perp) \times H^1_\beta(I_\perp)$, defined by

$$A(u, v) = (u_x, v)_\perp + (zu_y, v)_\perp, \quad \forall u, v \in H^1_\beta(I_\perp). \tag{2.17}$$

Let now $\tilde{u} \in V_{h,\beta}$ be an auxiliary projection of the solution u into $V_{h,\beta}$, defined by

$$A(u - \tilde{u}, \chi) = 0, \quad \forall \chi \in V_{h,\beta}. \tag{2.18}$$

The usual L_2-projection of u into $V_{h,\beta}$, being orthogonal, would satisfy (2.18).

2.2. **Convergence.** In this part we state and prove our main result: Theorem 2.3, or the convergence rate of the SG-method for the semidiscrete problem with weakly imposed boundary conditions.

Theorem 2.3 (error estimate in the triple norm)**.** *Assume that u and u_h satisfy (1.1) and (2.4), respectively. Let $u \in H^r(\Omega)$, $r \geq 1$, then there is a constant C such that,*

$$|||u_h - u|||_{\tilde{\beta}} \leq Ch^{r-1/2}\|u\|_r. \tag{2.19}$$

Proof. By adding first equation in (2.4) and (2.18) we get, using (1.1), that

$$\begin{aligned}((u_h-\tilde{u})_x,\chi)_\perp + (z(u_h-\tilde{u})_y,\chi)_\perp + (\varepsilon(u_h-\tilde{u})_z,\chi_z)_\perp \\ = -(u_x,\chi)_\perp - (zu_y,\chi)_\perp - (\varepsilon u_z,\chi_z)_\perp + (\varepsilon(u-\tilde{u})_z,\chi_z)_\perp \\ = 0 + (\varepsilon(u-\tilde{u})_z,\chi_z)_\perp.\end{aligned}$$

Let now $\chi = u_h - \tilde{u}$, then using the same argument as in the stability estimates we may write,

$$\begin{aligned}\frac{1}{2}\frac{d}{dx}\|u_h-\tilde{u}\|^2_{L_2(I_\perp)} + \frac{1}{2}\int_{\Gamma^+_\beta}(\mathbf{n}\cdot\beta)(u_h-\tilde{u})^2\,d\Gamma + \|\varepsilon^{1/2}(u_h-\tilde{u})_z\|^2_{L_2(I_\perp)} \\ \leq \frac{1}{2}\|\varepsilon^{1/2}(u_h-\tilde{u})_z\|^2_{L_2(I_\perp)} + \frac{1}{2}\|\varepsilon^{1/2}(u-\tilde{u})_z\|^2_{L_2(I_\perp)},\end{aligned}$$

or equivalently,

$$\begin{aligned}\frac{d}{dx}\|u_h-\tilde{u}\|^2_{L_2(I_\perp)} + \int_{\Gamma^+_\beta}(\mathbf{n}\cdot\beta)(u_h-\tilde{u})^2\,d\Gamma + \|\varepsilon^{1/2}(u_h-\tilde{u})_z\|^2_{L_2(I_\perp)} \\ \leq \|\varepsilon^{1/2}(u-\tilde{u})_z\|^2_{L_2(I_\perp)}.\end{aligned}$$

Now integrating over $x\in[0,L]$, implies that

$$\begin{aligned}\|(u_h-\tilde{u})(L,\cdot)\|^2_{L_2(I_\perp)} + \int_{\Gamma^+_{\tilde{\beta}}\setminus\Gamma_L}(\tilde{\mathbf{n}}\cdot\tilde{\beta})(u_h-\tilde{u})^2\,d\Gamma + \|\varepsilon^{1/2}(u_h-\tilde{u})_z\|^2_{L_2(\Omega)} \\ \leq \|\varepsilon^{1/2}(u-\tilde{u})_z\|^2_{L_2(\Omega)} + \|(u_h-\tilde{u})(0,\cdot)\|^2_{L_2(I_\perp)},\end{aligned}$$

where $\Gamma_L = \{\{L\}\times I_\perp\}$, further $u_h(0,\cdot)\in V_{h,\beta}$ and $\tilde{u}(0,\cdot)\in V_{h,\beta}$ are both approximating the initial data f, which by the uniqueness of the L_2-projection would mean that $u_h(0,\cdot)=\tilde{u}(0,\cdot)=f_h$. Thus recalling the definition of the $|||\cdot|||_{\tilde{\beta}}$ norm we have

$$|||u_h-\tilde{u}|||^2_{\tilde{\beta}} \leq \|\varepsilon^{1/2}(u-\tilde{u})_z\|^2_{L_2(\Omega)}.$$

Writing $u_h-u=(u_h-\tilde{u})+(\tilde{u}-u)$, the desired result follows from the following interpolation estimate: □

Proposition 2.4. *Let $h^2\leq\varepsilon(x,y)\leq h$, then there is a constant $\tilde{C}$ such that,*

$$|||u-\tilde{u}|||_{\tilde{\beta}} \leq \tilde{C}h^{r-1/2}\|u\|_r. \tag{2.20}$$

Proof. The proof is based on classical interpolation error estimates, see [7] and [9]: Let $u\in H^r(\Omega)$, them there exists an interpolant $\tilde{u}\in V_{h,\beta}$, of u and interpolation constants C_1 and C_2 such that

$$\begin{aligned}\|u-\tilde{u}\|_s &\leq C_1h^{r-s}\|u\|_r, \quad s=0,1\\ |u-\tilde{u}|_{\tilde{\beta}} &\leq C_2h^{r-1/2}\|u\|_r,\end{aligned}$$

where

$$|\varphi|_{\tilde{\beta}} = \left(\int_{\Gamma^+_{\tilde{\beta}}}\varphi^2(\tilde{\mathbf{n}}\cdot\tilde{\beta})\,d\Gamma\right)^{1/2}.$$

Now recalling the definition of $|||\cdot|||_{\tilde{\beta}}$ we have,

$$\begin{aligned}
|||u-\tilde{u}|||_{\tilde{\beta}}^2 &= \frac{1}{2}|u-\tilde{u}|_{\tilde{\beta}}^2 + \|\varepsilon^{1/2}(u-\tilde{u})_z\|_{L_2(\Omega)}^2 \\
&\le \frac{1}{2}|u-\tilde{u}|_{\tilde{\beta}}^2 + \|\varepsilon^{1/2}\|_{L_\infty(\Omega)}^2 \|(u-\tilde{u})_z\|_{L_2(\Omega)}^2 \\
&\le \frac{1}{2}|u-\tilde{u}|_{\tilde{\beta}}^2 + \left(\sup_{I_x\times I_y}\varepsilon\right)\|u-\tilde{u}\|_{H^1(\Omega)}^2 \\
&\le \frac{1}{2}C_2^2 h^{2r-1}\|u\|_r^2 + C_1^2\tilde{\varepsilon}h^{2r-2}\|u\|_r^2 \\
&\le Ch^{2r-1}\|u\|_r^2,
\end{aligned}$$

where in the last step we used $\tilde{\varepsilon} := \sup\varepsilon \le h$ and $C = \max(C_1^2, C_2^2/2)$. Letting now $\tilde{C} = C^{1/2}$ the proof is complete. □

Remark 2.2. Using the trace estimate and through embeddings between Sobolev and Besov spaces, we have for any fixed and small $\varepsilon_0 > 0$, the embedding relation $L_2(\partial\Omega) \subset H^{1/2-\varepsilon_0}(\Omega)$. Therefore the triple norm $|||\cdot|||_{\tilde{\beta}}$ is equivalent to a $H^{1/2-\varepsilon_0}$ norm. Now recalling, the Besov space notations for fractional derivatives, see also Bergh and Löfström [5], Theorem 2.3 states that:

$$\|e\|_{1/2} \le Ch^{r-1/2}\|u\|_r, \tag{2.21}$$

where $e = u - u_h$. Another way of seeing this is through Poincare inequality, see [2]. Hence, the L_2-error estimate for the standard finite element would be:

Proposition 2.5. *For $u \in H^r(\Omega)$, satisfying (1.1) and with u_h being the solution of (2.4), there is a constant $C = (\Omega, f)$ such that*

$$\|u-u_h\|_{L_2(\Omega)} \le Ch^{r-1}\|u\|_r. \tag{2.22}$$

Observe that in $C = (\Omega, f)$, the Ω dependence is because of $\varepsilon = \varepsilon(x,y)$, and the reason for f dependence is the assumed identity $u_h(0) := \tilde{u}(0)$.

3. THE STREAMLINE DIFFUSION METHOD

Proposition 2.5 gives the expected L_2-error estimate (2.22) for the standard finite element method for hyperbolic type problems: an optimal convergence rate of order $O(h^{r-1})$ when the exact solution $u \in H^r(\Omega)$. The corresponding rate for both elliptic and parabolic problems is of order $O(h^r)$. Usually, the modified Petrov-Galerkin method is used to improve this poor behavior of the SG-method for hyperbolic pde's. In the Petrov-Galerkin method the test and trial function spaces are different. Below this modification is suitably introduced in the streamline diffusion setting. A draw-back in problem (1.1) is that the hyperbolic nature yields to a bilinear form $A(u,v)$ which is not coercive (or V - elliptic), in the sense that a relation of the type

$$A(v,v) \ge C(r, I_\perp)\|v\|_{H^1(\Omega)}^2, \quad \forall v \in H_\beta^1(I_\perp),$$

simply fails to be valid. The streamline diffusion test functions having the form $v + \delta v_\beta$ would, automatically add an extra diffusion term, $\delta(v_\beta, v_\beta)$, to the variational

formulation which combined with $(v, -\varepsilon v_{zz}) = (\varepsilon v_z, v_z)$ term would give a, non-degenerate, fully diffusive equation, (x is interpreted as a time variable), with a diffusion term of order $O(\varepsilon)$, if $\delta \geq \varepsilon$. In the final discretized version, $\delta \sim h$.

Below we derive stability estimates for the continuous problem based on the SD variational formulation. The corresponding discrete version is then similar to that of the previous section and easily followed. For the proof of convergence rates for the SD-method we refer to [2].

Despite the common final form the mathematical treatment in streamline diffusion has no connection with the physically motivated add of artificial viscosity, as is customary in study of some fluid problems. Here the modified test function has the form: $v + \delta v_\beta$ with $\delta \geq \varepsilon, \beta = (z, 0), v_\beta = \beta \cdot \nabla_\perp v$ and $\nabla_\perp = (\partial/\partial y, \partial/\partial z)$, and v satisfying the boundary conditions in (1.1). Then multiplying the differential equation in (1.1) by $v + \delta v_\beta$ and integrating over $I_\perp$ yields,

$$\begin{aligned}(u_x + u_\beta - \varepsilon u_{zz}, v + \delta v_\beta)_\perp &= (u_x, v)_\perp + \delta(u_x, v_\beta)_\perp + (u_\beta, v)_\perp \\ &+ \delta(u_\beta, v_\beta)_\perp + (\varepsilon u_z, v_z)_\perp + \delta(\varepsilon u_z, (v_\beta)_z)_\perp = 0.\end{aligned} \tag{3.1}$$

To derive the basic stability estimate in this case, we let $v = u$ in (3.1) to obtain,

$$\begin{aligned}&\frac{1}{2}\frac{d}{dx}\|u\|_\perp^2 + \delta(u_x, u_\beta)_\perp + \frac{1}{2}\int_{\Gamma_\beta^+} (\mathbf{n} \cdot \beta) u^2 d\Gamma \\ &\qquad + \delta\|u_\beta\|_\perp^2 + \|\varepsilon^{1/2} u_z\|_\perp^2 + \delta(\varepsilon u_z, (u_\beta)_z)_\perp = 0.\end{aligned} \tag{3.2}$$

The inner product in the last term can be written as,

$$\begin{aligned}(\varepsilon u_z, (z u_y)_z)_\perp &= (\varepsilon u_z, z u_{yz})_\perp + (\varepsilon u_z, u_y)_\perp \\ &= \frac{1}{2}\frac{d}{dy}\left(\int_{I_\perp} \varepsilon z u_z^2 \, dy \, dz\right) - \frac{1}{2}\int_{I_\perp} \varepsilon_y z u_z^2 \, dy \, dz + (\varepsilon u_z, u_y)_\perp.\end{aligned}$$

Now since ε is independent of z the integrands above are odd functions in z and therefore their integrals over the symmetric interval I_z are identically zero, this is the basic consequence of assuming the symmetry condition (u is even in y and z), otherwise we had to keep these terms. Hence (3.2) can be written as:

$$\begin{aligned}&\frac{1}{2}\frac{d}{dx}\|u\|_\perp^2 + \delta(u_x, u_\beta)_\perp + \frac{1}{2}\int_{\Gamma_\beta^+} (\mathbf{n} \cdot \beta) u^2 d\Gamma \\ &\qquad + \delta\|u_\beta\|_\perp^2 + \|\varepsilon^{1/2} u_z\|_\perp^2 + \delta(\varepsilon u_z, u_y)_\perp = 0.\end{aligned} \tag{3.3}$$

Now we multiply the differential equation in (1.1) by δu_x, integrate over $I_\perp$ and perform an integration by parts to get,

$$\delta\|u_x\|_\perp^2 + \delta(u_x, u_\beta)_\perp + \delta(\varepsilon u_z, u_{xz})_\perp = 0. \tag{3.4}$$

Note that,

$$(\varepsilon u_z, u_{xz})_\perp = \frac{1}{2}\frac{d}{dx}\int_{I_\perp} \varepsilon u_z^2 \, dx_\perp - \frac{1}{2}\int_{I_\perp} \varepsilon_x u_z^2 \, dx_\perp. \tag{3.5}$$

Adding (3.3) and (3.4) and using (3.5) we have,

$$\begin{aligned}&\frac{1}{2}\frac{d}{dx}\|u\|_\perp^2 + \delta\|u_x + u_\beta\|_\perp^2 + \frac{1}{2}\int_{\Gamma_\beta^+} (\mathbf{n} \cdot \beta) u^2 \, d\Gamma + \|\varepsilon^{1/2} u_z\|_\perp^2 \\ &\qquad + \delta(\varepsilon u_z, u_y)_\perp + \frac{\delta}{2}\frac{d}{dx}\int_{I_\perp} \varepsilon u_z^2 \, dx_\perp - \frac{\delta}{2}\int_{I_\perp} \varepsilon_x u_z^2 \, dx_\perp = 0.\end{aligned} \tag{3.6}$$

We shall also use the following trivial inequality,

$$(\varepsilon u_z, u_y)_\perp \leq \frac{1}{2}\|\varepsilon^{1/2} u_z\|_\perp^2 + \frac{1}{2}\|\varepsilon^{1/2} u_y\|_\perp^2. \tag{3.7}$$

Now we need to make an additional symmetry assumption on the propagation of u on the transversal plane viz,

$$\|\varepsilon^{1/2} u_y\|_\perp \sim \|\varepsilon^{1/2} u_z\|_\perp. \tag{3.8}$$

Observe that $\varepsilon = \frac{1}{2}\sigma_{tr}(x,y) \sim 1/l$, where the mean free path l is an increasing function of x and y, (the justification of this phenomenon lies on the fact that we have a model starting with dense collisions which gradually, towards the penetration direction x, transfers to a particle distribution with rarefied character on leaving the physical domain). Thus ε is decreasing and $\varepsilon_x \leq 0$, hence

$$\int_{I_\perp} \varepsilon_x u_z^2 \, dx_\perp \leq 0. \tag{3.9}$$

Inserting (3.7-3.9) in (3.6) we get,

$$\begin{aligned} \frac{1}{2}\frac{d}{dx}\left(\|u\|_\perp^2 + \delta \int_{I_\perp} \varepsilon u_z^2 \, dx_\perp\right) + \frac{1}{2}\int_{\Gamma_\beta^+} u^2 (\mathbf{n}\cdot\beta) \, d\Gamma \\ + \delta\|u_x + u_\beta\|_\perp^2 + (1-\delta)\|\varepsilon^{1/2} u_z\|_\perp^2 \leq 0. \end{aligned} \tag{3.10}$$

Thus for sufficiently small $\delta \sim \sqrt{\varepsilon} << 1$, ($\delta < 1$ would suffice)

$$\frac{d}{dx}(\|u\|_\perp^2 + \delta \int_{I_\perp} \varepsilon u_z^2 \, dx_\perp) < 0, \tag{3.11}$$

and hence, $\left(\|u\|_\perp^2 + \delta \int_{I_\perp} \varepsilon u_z^2 \, dx_\perp\right)$ is strictly decreasing in x. As a consequence of this, we have $\forall x' \in [0, L]$,

$$\|u(x',\cdot)\|_{L_2(I_\perp)}^2 + \delta\|\varepsilon^{1/2} u_z(x',\cdot)\|_{L_2(I_\perp)}^2 \leq \|u(0,\cdot)\|_{L_2(I_\perp)}^2 + \delta\|\varepsilon^{1/2} u_z(0,\cdot)\|_{L_2(I_\perp)}^2,$$

and in particular we have the first stability estimate for the continuous SD-method:

$$\|u(L,\cdot)\|_{L_2(I_\perp)}^2 + \delta\|\varepsilon^{1/2} u_z(L,\cdot)\|_{L_2(I_\perp)}^2 \leq \|f\|_{L_2(I_\perp)}^2 + \delta\|\varepsilon^{1/2} f_z\|_{L_2(I_\perp)}^2. \tag{3.12}$$

Integrating (3.10) over $x' \in [0, L]$ we also get the second stability estimate:

Lemma 3.1. *Assuming (3.8) and with $\delta < 1$ we have the stability estimate*

$$|||u|||_{\tilde{\beta}}^2 + \delta\|u_x + u_\beta\|_{L_2(\Omega)}^2 \leq \bar{C}\left(\|f\|_{L_2(I_\perp)}^2 + \delta\|\varepsilon^{1/2} f_z\|_{L_2(I_\perp)}^2\right). \tag{3.13}$$

Remark 3.1: Observe that in deriving (3.13) from (3.10) we get the δ-terms $\delta\int_{I_\perp} \varepsilon u_z^2(L, x_\perp) \, dx_\perp = \delta\|\varepsilon^{1/2} u_z(L,\cdot)\|_{L_2(I_\perp)}^2$ and $(1-\delta)\|\varepsilon^{1/2} u_z\|_{L_2(I_x \times I_\perp)}^2$ adding up to $\sim \|\varepsilon^{1/2} u_z\|_{L_2(\Omega)}^2$, which is included in $|||u|||_{\tilde{\beta}}^2$. Further,

$$\frac{1}{2}\|u(L,\cdot)\|_{L_2(\Omega)}^2 + \frac{1}{2}\int_0^L \int_{\Gamma_\beta^+} (\mathbf{n}\cdot\beta) u^2 \, d\Gamma = \frac{1}{2}\int_{\Gamma_{\tilde{\beta}}^+} (\mathbf{n}\cdot\tilde{\beta}) u^2 \, d\Gamma, \tag{3.14}$$

which is also included in $|||u|||_{\tilde{\beta}}^2$. Thus the assertion of Lemma 3.1, is simply,

$$\delta\|u_x + u_\beta\|_{L_2(\Omega)}^2 + \|\varepsilon^{1/2}u_z\|_{L_2(\Omega)}^2 + \frac{1}{2}\int_{\Gamma_{\tilde{\beta}}^+}(\mathbf{n}\cdot\tilde{\beta})u^2\, d\Gamma \leq \bar{C}\left(\|f\|_{L_2(I_\perp)}^2 + \delta\|\varepsilon^{1/2}f_z\|_{L_2(I_\perp)}^2\right),$$

where $\bar{C} \sim \frac{1}{2(1-\delta)} \sim \frac{1}{2(1-h)} < 1$, for $h < 1/2$. Comparing this estimate with the continuous counterpart of the second assertion, i.e. (2.7), of Lemma 2.1 we get,

$$\|u_x + u_\beta\|_{L_2(\Omega)} \leq \bar{C}\|\varepsilon^{1/2}f_z\|_{L_2(I_\perp)}. \tag{3.15}$$

Using the equation this yields,

$$\|\varepsilon u_{zz}\|_{L_2(\Omega)} \leq \bar{C}\|\varepsilon^{1/2}f_z\|_{L_2(I_\perp)}. \tag{3.16}$$

The estimate (3.16) states that if $\varepsilon = O(1)$ then the solution is regularized in the sense that $f \in H^1_{\sqrt{\varepsilon}}(I_\perp)$ implies $u \in H^2_\varepsilon(\Omega)$. However, this is obviously affected by small ε values and, in particular, is distorted when $\varepsilon = \frac{1}{2}\sigma_{tr}(x,y) \to 0$.

Remark 3.2. The discrete version is now obtained by replacing u by a suitable u_h, having the desired approximation properties, see [2]. The corresponding semidiscrete convergence analysis would improve the results of Section 2 (Theorem 2.3 and Propositions 2.4 and 2.5) by $O(h^{1/2})$. We emphasise that, the general convergence studies for the SD-method shows that the suitable so called *compatibility relations* are $\delta \sim h$ and $\varepsilon \sim h^2$. Here, to be concise we skip deriving these convergence rates and refer the reader to [2] for further details.

4. THE FULLY DISCRETE PROBLEM

In this section, we derive the algorithms corresponding to the standard Galerkin and streamline diffusion methods for $I_\perp$ combined with discontinuous Galerkin, backward-Euler and Cranck-Nicolson methods for the penetration interval I_x.

The approximation techniques in Sections 2 and 3 are designed for discretizations in the transversal variable $x_\perp = (y,z)$. Of course we could include the penetration variable x, in this procedure as an additional space variable, as it is (see the analysis in [2]) where full discretizations are made in all three variables using both streamline diffusion and discontinuous Galerkin methods. However, to efficiently determine the beam intensity at different cross section discretizations in the penetration variable x, needs separate and special attention. To this approach we treat the penetration variable x as being a time variable in similar time dependent equations. Thus, in extending our semidiscrete algorithms to a higher dimensional case containing also discretizations in x, we consider the time discretization schemes for I_x, such as the discontinuous Galerkin, presented in [2], and backward Euler and Cranck-Nicolson schemes which are briefly introduced in the combined algorithms below:

We split the continuous SD variational formulation (3.1) according to:

$$a(u,v) = (u_x,v)_\perp + \delta(u_\beta,v_\beta)_\perp + (\varepsilon u_z,v_z)_\perp + \delta(\varepsilon u_z,(v_\beta)_z)_\perp \tag{4.1}$$

$$b(u,v) = \delta(u,v_\beta)_\perp + (u,v)_\perp, \tag{4.2}$$

and rewrite the problem (3.1) as finding a solution $u \in H^1_\beta(I_\perp)$ of,

$$b(u,v) + a(u,v) = 0, \quad \forall v \in H^1_\beta(I_\perp). \tag{4.3}$$

We subsequently use the finite dimensional subspace, $V_{h,\beta}$ of $H^1_\beta(I_\perp)$ and represent the discrete solution u_h by a separation of variables viz:

$$u_h(x,y,z) = \sum_{i=1}^{M} \xi_i(x)\phi_i(y,z), \tag{4.4}$$

where $M \sim 1/h$. Now we let, $v = \phi_j$ for $j = 1,\ldots,M$, and insert (4.4) into the semidiscrete counterpart of (3.1) to obtain,

$$\sum_{i=1}^{M} \xi_i^{'}(x)b(\phi_i,\phi_j) + \sum_{i=1}^{M} \xi_i(x)a(\phi_i,\phi_j) = 0, \qquad j = 1,\ldots,M. \tag{4.5}$$

In the matrix form (4.5) may be represented by, $B\xi^{'}(x) + A\xi(x) = 0$, where, $B = (b_{i,j})$ with $b_{i,j} = b(\phi_i,\phi_j)$ and $A = (a_{i,j})$ with $a_{i,j} = a(\phi_i,\phi_j)$. It is easy to verify that for small δ the matrix B, being positive definite, is invertible and therefore we can reformulate (4.5) as,

$$\xi'(x) + \bar{A}\xi(x) = 0, \tag{4.6}$$

where $\bar{A} = B^{-1}A$.

The equations above can easily be implemented for usual finite element test functions (streamlines with $\delta = 0$). In this manner our algorithm can be easily used to compare the SG and SD methods.

Now a fully discrete scheme is obtained by also discretizing (4.6) in the x direction. Below we combine both SG and SD-methods, for discretization in $x_\perp$, with the most common time discretization techniques applied to our x variable. To achieve the most general results on the number of scheme combinations for the x discretization we extract them from Pade approximations of the general form, $U^{n+1} = E_{\mu\nu}U^n$ for $n \geq 0$, where $E_{\mu\nu} = r_{\mu\nu}(\bar{A})$. Here, $r_{\mu\nu}(x) = \frac{\eta_{\mu\nu}(x)}{d_{\mu\nu}(x)}$ with,

$$\eta_{\mu\nu}(x) = \sum_{j=0}^{\nu} \frac{(\mu+\nu-j)!\nu!}{(\mu+\nu)!j!(\nu-j)!}(-x)^j, \tag{4.7}$$

$$d_{\mu\nu}(x) = \sum_{j=0}^{\mu} \frac{(\mu+\nu-j)!\mu!}{(\mu+\nu)!j!(\mu-j)!}x^j. \tag{4.8}$$

For instance $r_{01}(x) = 1 - x$ corresponds to forward Euler, $r_{10}(x) = 1/(1+x)$ to backward Euler whereas r_{11} to Crank-Nicolson scheme. Some of these for instance can be seen in full below,

$$\left(\frac{U_h^n - U_h^{n-1}}{k_n}\right) + \bar{A}U_h^n = 0, \quad \text{backward Euler,} \tag{4.9}$$

$$\left(\frac{U_h^n - U_h^{n-1}}{k_n}\right) + \bar{A}\left(\frac{U_h^n + U_h^{n-1}}{2}\right) = 0, \quad \text{Crank Nicolson.} \tag{4.10}$$

Other such choices will easily provide comparisons for alternative methods.

5. NUMERICAL EXAMPLES

To justify the theoretical estimates of Sections 2 and 3 we present some numerical examples testing the convergence rates of both the SG and SD. To this approach we combine SG and SD methods with three different cases of discretizations in I_x: namely backward Euler, Crank Nicolson and discontinuous Galerkin. The

implementations are performed over five different initial conditions: cone, cylinder, Maxwellian, hyperbolic and modified Dirac, all approximating our data: the Dirac δ function.

We split the problem into two steps. First we discretize the two dimensional $I_\perp = I_y \times I_z$ domain by means of piecewise linear approximations cG(1), and establish a mesh there in order to obtain a semidiscrete solution and then we apply one of the three schemes, backward Euler, Crank-Nicolson or discontinuous Galerkin to step advance in the x direction. Of course one can easily implement higher order elements if so desired. Our cG(1) basis functions have the form, $\phi_i = a_1 y + a_2 z + a_3$.

Notice that, in some special cases (for instance, for $\varepsilon = \varepsilon(x)$, see [8]) the closed form exact solution of (1.1) is given by,

$$u(x,y,z) = \frac{2\sqrt{3}}{\pi k x^2} e^{-4\left[3(y/x)^2 - 3(y/2)z + z^2\right]/(kx)}. \tag{5.1}$$

This allows us to draw some limited comparisons in terms of the actual error. In addition to being an extremely limited case, the reason for not being able to take full advantage of knowing the exact solution (5.1) is the fact that it displays strong singularities near the origin. Obviously the final solution depends on initial conditions and therefore it is not correct to compare (5.1) with the solutions we obtain numerically since the underlying initial conditions were not the same to start with. For instance we can not numerically provide an initial data of the form of a Dirac δ function. We instead use our five different types of *computable initial conditions*, each approximating the Dirac δ function (in the L_1 sense), for comparison purposes. The reason for using all these different examples is exactly that dependence of the solution on initial conditions. We want to see how the initial conditions can affect our estimates on convergence established in Sections 2 and 3. In the results that follow we show the convergence rates (and hopefully speedup) in obtaining the same solution from the same initial condition under both SG and SD discretizations.

In the tables that follow we display errors: the comparisons (differences) between solutions obtained from all the initial conditions used under both types of finite elements. We particularly calculate the L_1, L_2, L_∞ and $\tilde{L}_2$, (defined below), norms of the difference for each such approximate solution and its highest order approximation found (through the finest mesh used). The $\tilde{L}_2$ which is based on edge midpoints (instead of node) evaluations. This norm is defined as,

$$\|\varphi\|_{\tilde{L}_2} = \left(\frac{1}{3} \sum_{\tau_i} |\tau_i| \sum_{j=1}^{3} \left(\varphi(\zeta_j^i)\right)^2 \right)^{1/2}, \tag{5.2}$$

where τ_i are the triangles in the mesh and ζ_j^i denote the midpoints of the edges of τ_i.

The calculations are performed on an **Origin 2000** supercomputer with varying number of processors used at each running occasion. A total of almost 200 supercomputer hours were used for all the necessary computations. The finest mesh used (for at least some of the examples) for our domain Ω has a step size of $h = .025$ in the y and z variables and step size $k = .0005$ in the x variable. This creates a total of 6561000 nodes (in three dimensions) and in particular 6561 $(= 81 \times 81)$ nodes (in two dimensions) for each 'exact' solution which will be used to calculate the norms with solutions due to lesser number of nodes. The values in the tables

are provided for $\epsilon = .05$ and $\delta = .05$. These calculations are performed under all five types of considered initial conditions under each case of finite elements, under all three types of time increment methods and finally under 3 different mesh sizes. This gives a total of, $5 \times 2 \times 3 \times 3 = 90$ different solution evaluations. The 'exact' solution for these comparisons which has a step size of $h = .1$ in the y and z axes, is denoted by u^*. We let $e_h^* = u^* - U_h$, where U_h denotes the approximate solution for a mesh with step size h on the (y, z) space. All solutions are provided for $x = 1$ and therefore the norms are calculated at this value of x.

Some of the initial conditions used in calculating the values in the tables can be seen in Figure 1. In Figure 2 the approximate solution is displayed for a Dirac type of initial condition in the finest mesh used.

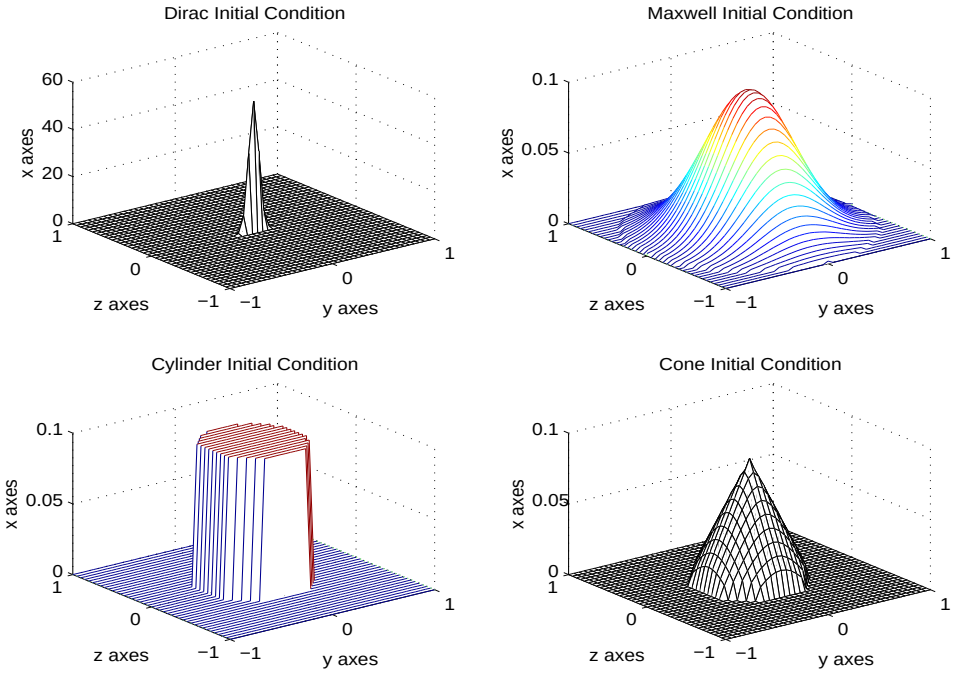

FIGURE 1. Some of the initial conditions used.

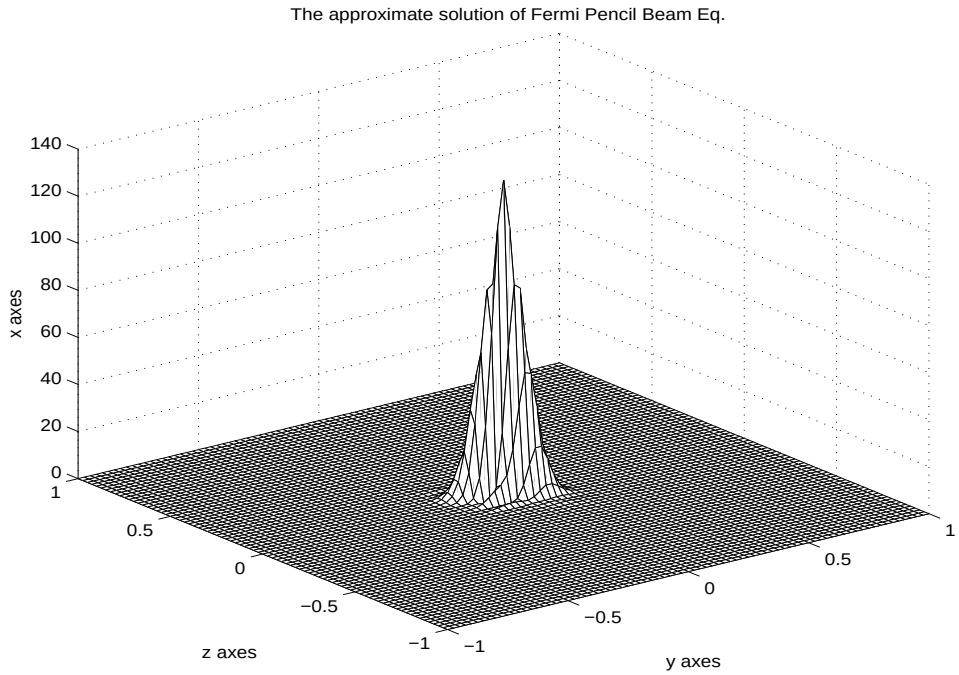

FIGURE 2. An example of a solution. The Dirac initial condition is used with $\epsilon = .002$, $h = .025$ and $k = .0005$.

Backward Euler

Galerkin elements

	Cone e^*_{4h}— e^*_{2h}	Cylinder e^*_{4h}—e^*_{2h}	Dirac e^*_{4h}—e^*_{2h}	Hyperbolic e^*_{4h}— e^*_{2h}	Maxwellian e^*_{4h}—e^*_{2h}
L_1	4.429—2.937	6.057—4.930	27.92—10.28	1.828—.911	4.343—2.679
L_2	3.446—2.074	4.766—3.485	26.79—8.44	1.556—.627	3.330—1.845
L_∞	4.766—3.135	6.620—5.306	48.69—16.99	2.245—.904	4.073—2.636
$\tilde{L}_2$	1.152—.471	1.533—.797	13.63—1.806	.648—.139	1.233—.425

Streamline Diffusion elements

	Cone e^*_{4h}—e^*_{2h}	Cylinder e^*_{4h}—e^*_{2h}	Dirac e^*_{4h}—e^*_{2h}	Hyperbolic e^*_{4h}— e^*_{2h}	Maxwellian e^*_{4h}—e^*_{2h}
L_1	4.414—2.873	5.661—4.753	27.75—9.676	1.846—.951	4.208—2.612
L_2	3.207—2.037	4.412—3.407	27.16—8.522	1.516—.641	3.221—1.799
L_∞	4.332—2.877	6.006—4.941	50.93—15.22	2.081—.839	4.189—2.460
$\tilde{L}_2$	1.104—.457	1.461—.770	13.33—1.801	.637—.149	1.187—.413

Crank-Nicolson

Galerkin elements

	Cone e^*_{4h}— e^*_{2h}	Cylinder e^*_{4h}— e^*_{2h}	Dirac e^*_{4h}— e^*_{2h}	Hyperbolic e^*_{4h}— e^*_{2h}	Maxwellian e^*_{4h}— e^*_{2h}
L_1	.442—.295	.604—.495	27.99—10.32	.183—.091	.454—.257
L_2	.345—.209	.478—.351	26.93—8.473	.156—.063	.356—.180
L_∞	.478—.315	.664—.532	49.12—17.27	.225—.091	.469—.270
$\tilde{L}_2$	.115—.047	.153—.080	13.73—1.814	.065—.014	.122—.041

Streamline Diffusion elements

	Cone e^*_{4h}— e^*_{2h}	Cylinder e^*_{4h}—e^*_{2h}	Dirac e^*_{4h}— e^*_{2h}	Hyperbolic e^*_{4h}— e^*_{2h}	Maxwellian e^*_{4h}— e^*_{2h}
L_1	.415—.288	.566—.477	27.80—9.697	.185—.095	.426—.254
L_2	.321—.204	.441—.341	27.33—8.527	.152—.064	.332—.178
L_∞	.434—.286	.602—.492	51.50—15.24	.208—.084	.426—.245
$\tilde{L}_2$	.110—.045	.146—.077	13.44—1.806	.063—.015	.117—.040

Discontinuous Galerkin

Galerkin elements

	Cone e^*_{4h}— e^*_{2h}	Cylinder e^*_{4h}—e^*_{2h}	Dirac e^*_{4h}— e^*_{2h}	Hyperbolic e^*_{4h}— e^*_{2h}	Maxwellian e^*_{4h}— e^*_{2h}
L_1	.420—.311	.581—.584	29.75—11.56	.202—.088	.428—.275
L_2	.303—.237	.428—.413	29.04—9.809	.161—.061	.309—.200
L_∞	.404—.498	.552—.835	52.54—21.13	.224—.089	.429—.417
$\tilde{L}_2$	.110—.051	.146—.091	13.40—2.065	.064—.012	.117—.043

Streamline Diffusion elements

	Cone e^*_{4h}— e^*_{2h}	Cylinder e^*_{4h}— e^*_{2h}	Dirac e^*_{4h}— e^*_{2h}	Hyperbolic e^*_{4h}— e^*_{2h}	Maxwellian e^*_{4h}— e^*_{2h}
L_1	.428—.264	.590—.488	30.19—10.51	.188—.090	.437—.247
L_2	.296—.220	.411—.377	29.24—10.17	.152—.067	.304—.193
L_∞	.401—.455	.554—.774	53.34—19.71	.221—.100	.428—.382
$\tilde{L}_2$	.110—.049	.145—.087	13.28—2.068	.063—.014	.117—.042

In the tables we see the convergence of each scheme as the step size is reduced. More importantly however we detect a slight improvement over using SD from SG in terms of the consistent decrease in the respective errors. Depending on the initial condition used the rates of this decay vary.

In figures studies on two of initial data (Dirac and Maxwellian) are presented in some detail, while the remaining cases (because of space limitations) are shown rather briefly. More specifically in Figures 3-6 we consider Dirac and Maxwellian studies and look at slices of the domain Ω and the differences between the 'exact'

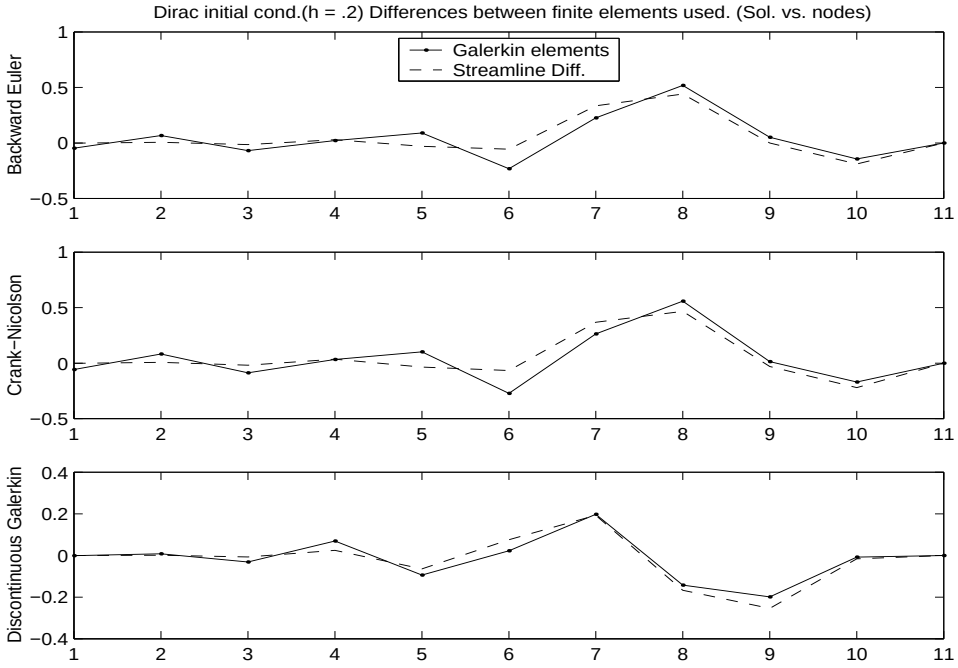

FIGURE 3. Galerkin vs. Streamline elements for Dirac initial condition at $h = .2$ for the slice, $-1 \leq y \leq 1$ at $z = -.9$.

and approximate solutions over all three cases of time discretization schemes, thus providing us a 'local' picture of the variation depicted in the tables. Further we provide a fuller view of this variation, for all considered initial data cases, over the whole domain in Figures 7- 11. For each initial data in these figures we explore the effects of the SG and SD solutions ONLY under the case of backward Euler time discretization where particular emphasis is given on plotting the cumulative L_1 error of the schemes. The computational parameters that are used depend on the theoretical results presented in Sections 2 and 3. For instance ε must be chosen to be small and given such a choice we take $h^2 \sim \varepsilon$, also $\delta \sim h$. Specifically Figures 7-11 were produced for values of $\epsilon = .005$ and $h = .1$ which also determines the finest mesh used for our 'exact' solution. The value of δ is taken as $\delta = h/2$ for these examples. It is clear that many other similar values can easily be implemented and can also display, with varying rates of convergence, the expected theoretical estimates. The time increment was chosen as $k = h^2$.

In Figure 7 we see the improvement due to SD over SG for a Dirac type of initial condition. In particular we see that the error of using SD is reduced by $1/5$ over the error of SG. This behavior is maintained for a Maxwellian type of initial condition as can be seen in Figure 8. Here the error for using SD is reduced approximately by $1/6$ over using SG. Similar such results are displayed in Figures 9-11. For instance for a cone type of initial condition and a value of $\epsilon = .04$ (for variety purposes), we observe a $1/6$ improvement of the error due to SD over SG.

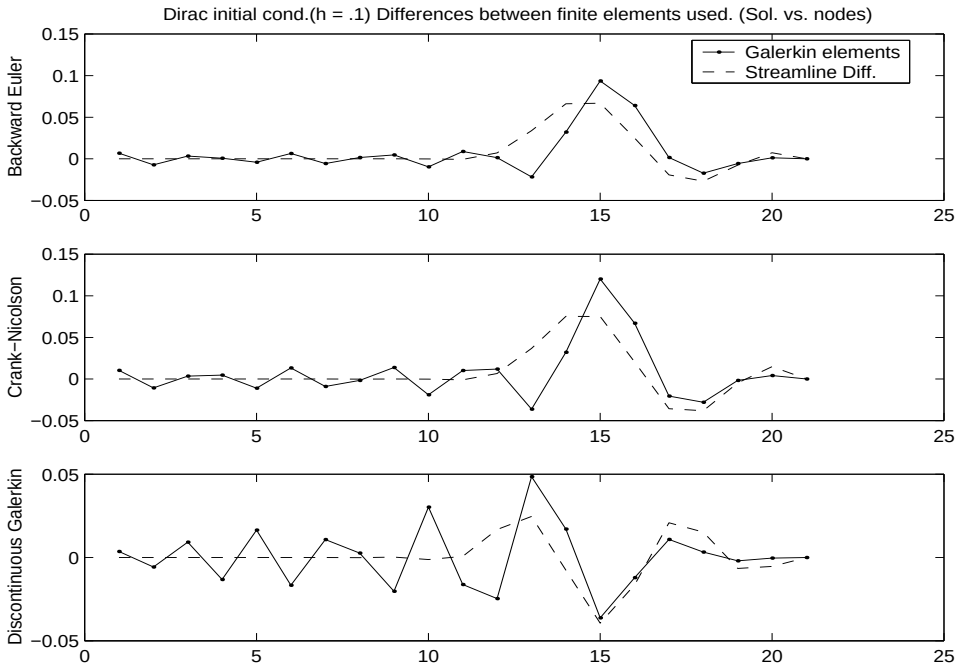

FIGURE 4. Galerkin vs. Streamline elements for Dirac initial condition at $h = .1$ for the slice, $-1 \leq y \leq 1$ at $z = -.9$.

6. CONCLUSIONS

We have shown stability and convergence estimates for SG and SD methods. Subsequent simple numerical examples were carried out to further illustrate the results under different cases of initial conditions. In theory the SD converges by a factor of $h^{r-1/2}$ (compared with SG which converges with a factor of h^{r-1}) for functions in $H^r(\Omega)$. Our examples correspond to $r = 1$, since we use linear basis functions. For such simple examples it is virtually impossible to calculate the exact estimates as required for instance in Proposition 2.4, since the $|||\cdot|||_{\tilde{\beta}}$ norm is not easily computable. Therefore, tables are constructed for L_p, $p = 1, 2, \infty$ and $\tilde{L}_2$ norms whereas in the figures we compared the simpler L_1 norms of the errors for the SD and SG schemes.

The theoretical estimates (Sections 2 and 3) are much harder to detect numerically in our experiments since, as we previously remarked, we are not using the exact solution of the Fermi equation but only an approximation of it in the finest mesh we can produce and subsequently calculate the errors from it. Also we do not directly evaluate the $|||\cdot|||_{\tilde{\beta}}$ but only an L_1 norm. However even under these circumstances the speed up of SD over SG is evident and as we have shown it depends on the type of initial data used, as expected.

In summary we have considered a simplest possible degenerate type equation. Our objective is to extend the approximation techniques for the non-degenerate equations to a degenerate case. In a forthcoming paper we shall extend our studies to a more realistic, three dimensional, model problem.

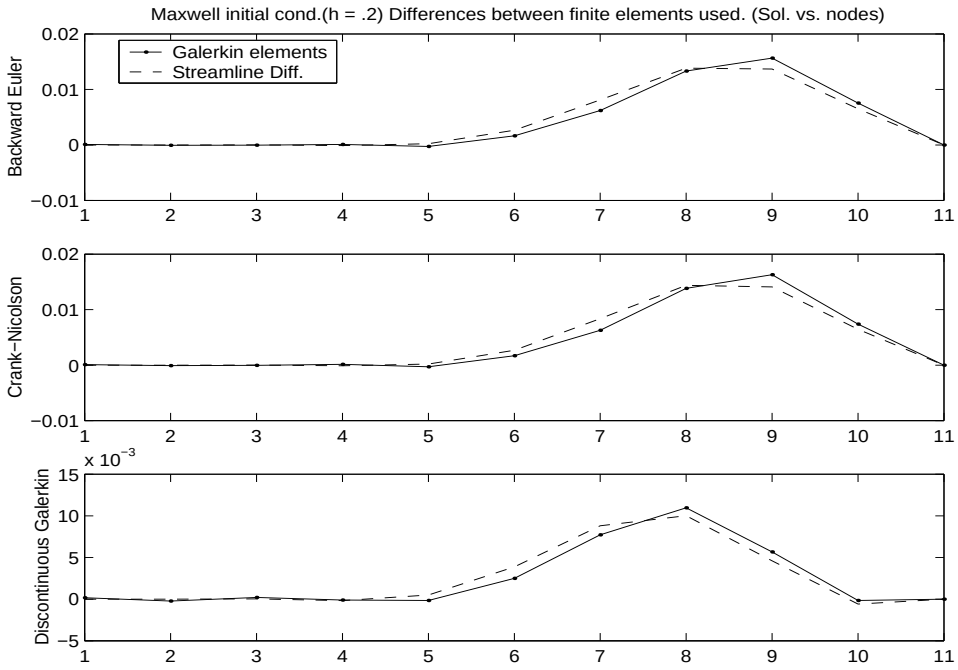

FIGURE 5. Galerkin vs. Streamline elements for Maxwell initial condition at $h = .2$ for the slice, $-1 \leq y \leq 1$ at $z = -.9$.

Acknowledgements: A. Sopasakis is on a European Union's TMR post-doc program led by the kinetic theory group at the Mathematics department of Chalmers University of Technology and Göteborg University.

REFERENCES

1. R. A. Adams, *Sobolev spaces*, Academic Press, New York, 1975.
2. M. Asadzadeh, *Streamline diffusion methods for Fermi and Fokker-Planck equations*, Transport Theory Statist. Phys. **26** (1997), no. 3, 319–340.
3. ———, *A posteriori error estimates for the Fokker-Planck and Fermi pencil beam equations*, Math. Models Meth. Appl. Sci. **10** (2000), 737–769.
4. ———, *Characteristic Methods for Fokker-Planck and Fermi pencil beam equations*, in Rarefied Gas Dynamics, eds. R. Brun, R. Campargue, R. Gatignol and J.-C. Lengrand (Cépaduès Éditions, 1999), vol. 2, pp. 202–212.
5. J. Bergh and J. Löfsröm, *Interpolation Spaces*, Springer-Verlag, 1976.
6. C. Börgers and E. W. Larsen, *Asymptotic derivation of the fermi pencil-beam approximation*, Nucl. Sci. Eng. **123** (1996), 343–357.
7. S. C. Brenner and L. R. Scott, *The Mathematical Theory of Finite Element Methods*, Springer-Verlag, 1994.
8. D. Jette, *Electron dose calculations using multiple-scattering theory. A new theory of multiple-scattering*, J. Med. Phy. **23** (1996), 459–476.
9. C. Johnson, *Numerical solution of partial differential equations by the finite element method*, Studentlitteratur, 1991.

DEPARTMENT OF MATHEMATICS, CHALMERS UNIVERSITY OF TECHNOLOGY AND GÖTEBORG UNIVERSITY, SE–412 96, GÖTEBORG, SWEDEN
E-mail address: mohammad@math.chalmers.se
E-mail address: sopasak@math.chalmers.se

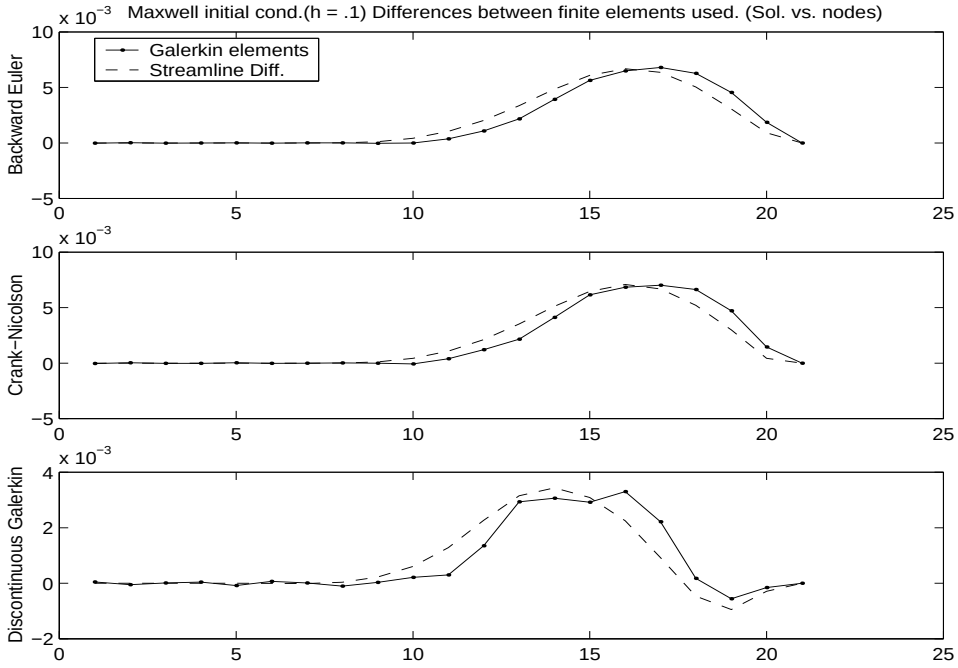

FIGURE 6. Galerkin vs. Streamline elements for Maxwell initial condition at $h = .1$ for the slice, $-1 \leq y \leq 1$ at $z = -.9$.

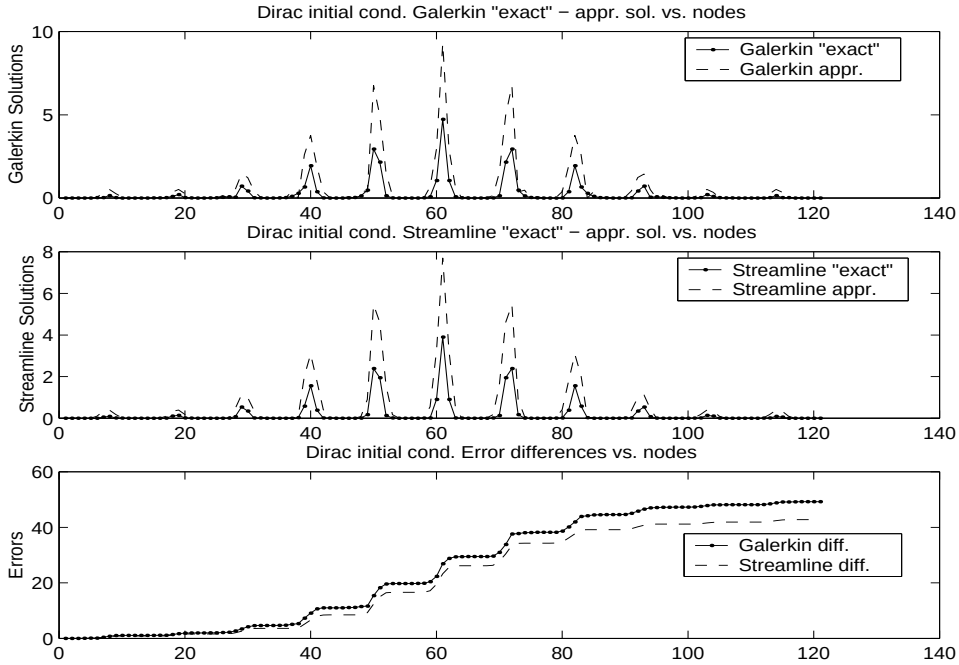

FIGURE 7. L_1 cumulative error vs nodes for SG and SD for Dirac. The solutions at $x = 1$ are found for $h = .2$.

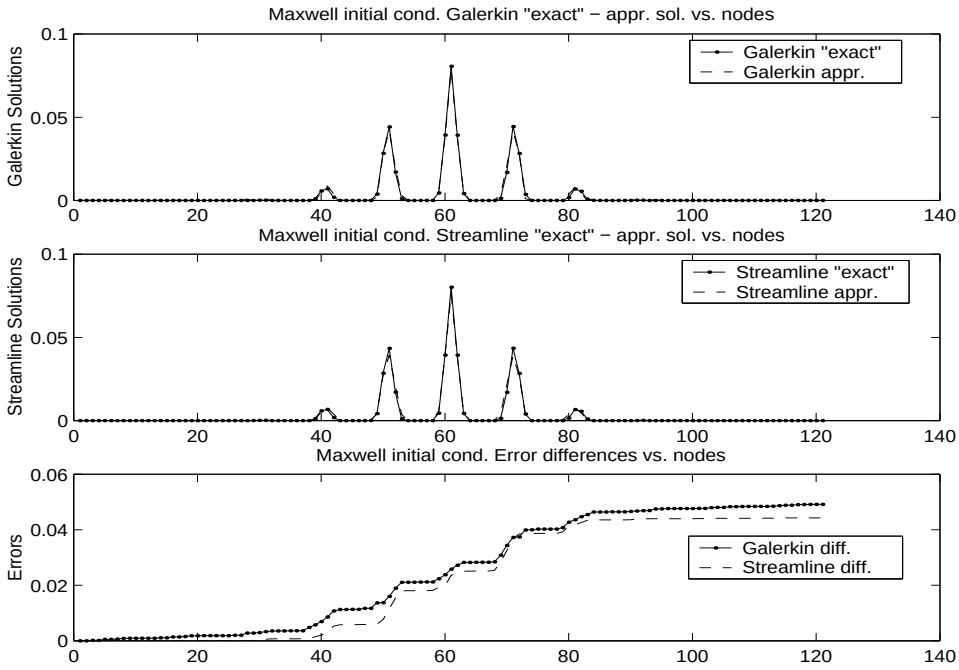

FIGURE 8. L_1 cumulative error vs nodes for SG and SD for Maxwell. The solutions at $x = 1$ are found for $h = .2$.

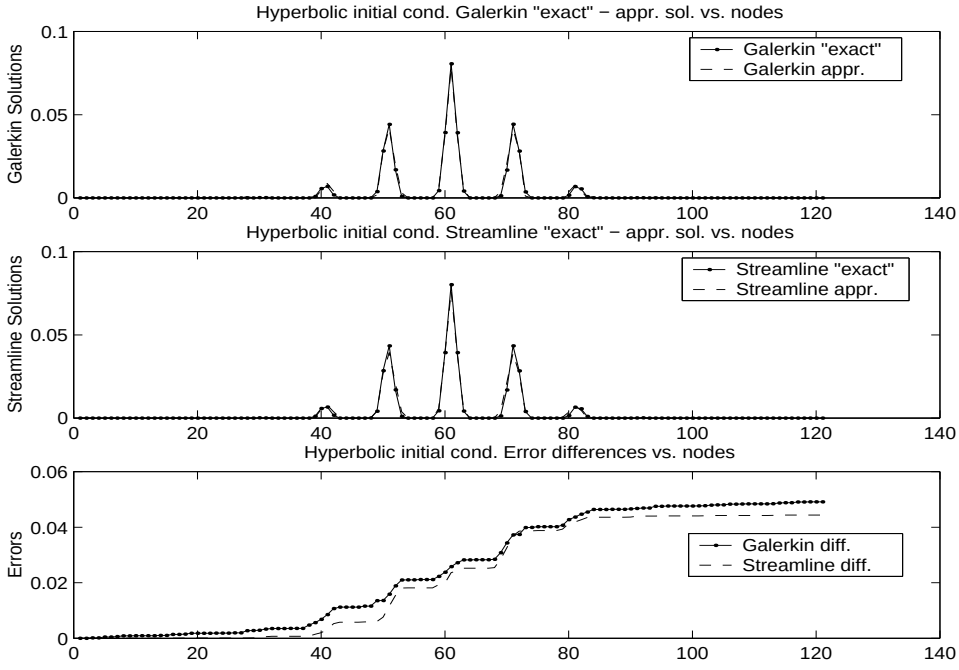

FIGURE 9. L_1 cumulative error vs nodes for SG and SD for hyperbolic. The solutions at $x = 1$ are found for $h = .2$.

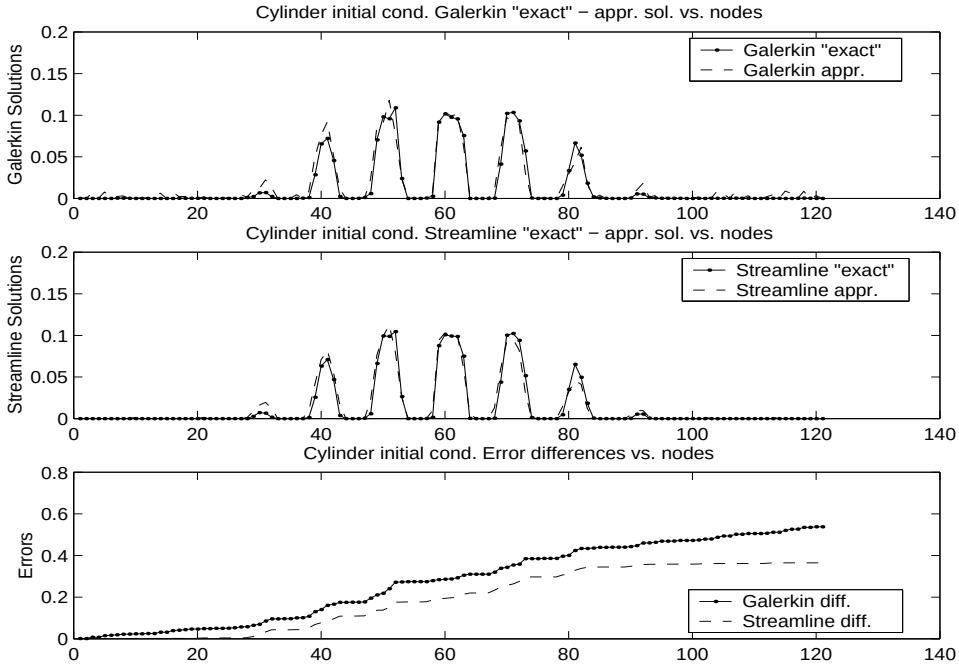

FIGURE 10. L_1 cumulative error vs nodes for SG and SD for cylinder. The solutions at $x = 1$ are found for $h = .2$.

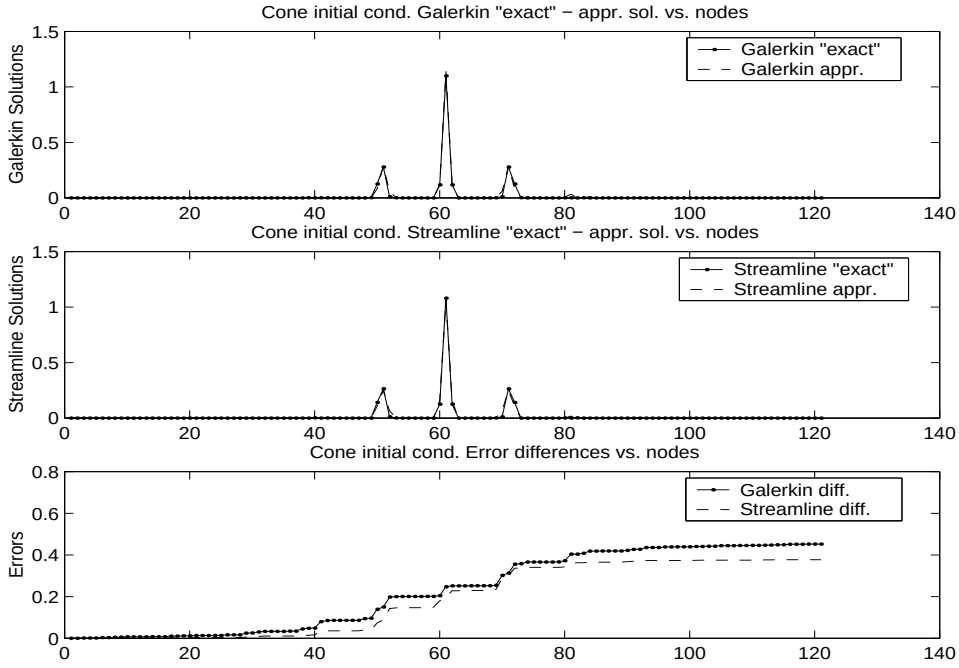

FIGURE 11. L_1 cumulative error vs nodes for SG and SD for cone data. The solutions at $x = 1$ are found for $h = .2$.